Electronic Supplementary Material (ESI) for Physical Chemistry Chemical Physics.

Supporting information for: Influence of Orientation Mismatch on Charge Transport Across Grain Boundaries in Tri-isopropylsilylethynyl (TIPS) Pentacene Thin Films†

Florian Steiner,[a‡] Carl Poelking,[b‡] Dorota Niedzialek,[a] Denis Andrienko,[b] and Jenny Nelson*[a]

[a] *Department of Physics and Centre for Plastic Electronics, Imperial College London, London SW7 2AZ; E-mail: jenny.nelson@imperial.ac.uk*
[b] *Max Planck Institute for Polymer Research, Ackermannweg 10, 55128 Mainz.*
† Electronic Supplementary Information (ESI) available. See DOI: 10.1039/b000000x/
‡ These authors contributed equally to this work.

Supporting Information

A A. Force-Field of TIPS-P

For atomistic molecular-dynamics simulations a force-field specific to TIPS-P is developed. The OPLS-AA force-field

$$E = \sum_{i<j} 4\varepsilon_{ij}\left[\left(\frac{\sigma_{ij}}{r_{ij}}\right)^{12} - \left(\frac{\sigma_{ij}}{r_{ij}}\right)^{6}\right] + \sum_{i<j}\frac{1}{4\pi\varepsilon_r\varepsilon_0}\frac{q_i q_j}{r_{ij}}$$
$$\sum_b \frac{1}{2}K_b(b-b_0)^2 + \sum_\theta \frac{1}{2}K_\theta(\theta-\theta_0)^2 \quad (1)$$
$$\sum_\xi \frac{1}{2}K_\xi(\xi-\xi_0)^2 + \sum_n c_n cos^n(\phi-\phi_0)$$

was adopted where the first two terms represent non-bonding interactions (Lennard-Jones and Coulomb potentials) and the last four terms relate to bonding interactions (bond, angle, improper dihedrals and dihedrals)[1]. For TIPS-P we define seven different atom identities that refer to OPLS-AA atom types (see Table 1).

atom identity	opls number	atom type	in forcefield
Cxx	opls_135	alkane CH3	CT
Cx	opls_136	alkane CH2	CT
Hx or Hxx	opls_140	alkane H	HC
CAx	opls_145	benzene C	CA
HAx	opls_146	benzene H	HA
CTx	opls_925	alkyne	CZ
Six	opls_966	silicon	SI

Table 1 Symbols used in Figure 1 according OPLS-AA number and atom type. x stands for an arbitrary integer.

A Mulliken population analysis was conducted to compute atomic charges. The molecular geometry was optimised and atomic charges were calculated with hybrid density functional theory employing the hybrid functional B3LYP and a 6-311g(d,p) basis set. The results are given in Table 2. For all carbon and hydrogen atoms masses and Lennard-Jones parameters are taken from the OPLS-AA force-field. For silicon we use the Lennard-Jones parameters provided in reference[2] (SI: $\varepsilon_{ii} = 0.398\,\mathrm{kJ/mol}$ and $\sigma_{ii} = 0.4435\,\mathrm{nm}$).

In the following we discuss specifications for bond types, angle types and dihedral types (see Tables 3, 4 and 5. Parameters for bonds, angles and dihedrals between carbon and hydrogen atoms can be found in the OPLS-AA database and are not discussed here. Parameters concerning silicon are provided in the tables mentioned above.

Since silicon is a four-bonding atom like carbon, we consider for angles and dihedrals containing silicon OPLS-AA parameters for alkanic carbon (CT) or rely on previous parameters provided by Guilbert and co-workers[3] (see Tables 4 and 5). In terms of bonds, reference[3] provides the equilibrium bond length b_0 and the force constant K_b for SI-CT. In contrast, the specifications of the bond SI-CZ are unknown.

We geometrically optimise TIPS-P with hybrid density functional theory (B3LYP/6-311g(d,p)). Accordingly, we iteratively vary the equilibrium bond length and the force constant of the SI-CZ bond in the force-field until all bond lengths agree in the molecular geometries from density functional theory and molecular mechanics. The result is provided in Table 3. Thereafter, the force-field was tested on a 3 x 3 TIPS-P supercell. We found that the supercell and the molecular geometries were stable.

atom identity	Mulliken charge (C)	atom identity	Mulliken charge (C)
CA6	-0.037903	C61	-0.280104
CA5	-0.024736	H61	0.107321
CAi	-0.017368	H62	0.104415
CAh	-0.031665	H63	0.104267
CA4	0.015652	C62	-0.281669
CAj	0.014919	H64	0.101288
CAk	-0.050873	H65	0.100655
CA3	-0.062843	H66	0.118958
CA2	-0.068552	C41	-0.281219
HA2	0.090358	H41	0.105783
CA1	-0.091045	H42	0.104058
CAm	-0.088084	H43	0.107806
CAl	-0.061955	C42	-0.280412
HA4	0.133049	H44	0.117911
HAj	0.117454	H45	0.100254
HA1	0.095289	H46	0.106212
HAm	0.095368	C51	-0.287312
HAl	0.084265	H51	0.110784
CA7	-0.011951	H52	0.102495
CA8	0.015823	H53	0.110066
CAg	-0.021739	C52	-0.285191
HA8	0.123179	H54	0.116829
CAf	0.010026	H55	0.102296
HAf	0.137156	H56	0.105284
CA9	-0.053162	C3	-0.50675
CAa	-0.063648	H3	0.14054
CAe	-0.063644	C31	-0.276603
CAb	-0.0888	H31	0.104923
HAa	0.086942	H32	0.106576
CAd	-0.068506	H33	0.105829
CAc	-0.090646	C32	-0.291701
HAb	0.095537	H34	0.104434
HAd	0.08922	H35	0.10226
HAc	0.09533	H36	0.118824
CT1	0.018347	C21	-0.279957
CT2	-0.533583	H21	0.099471
Si1	1.248732	H22	0.099909
C1	-0.501642	H23	0.123337
H1	0.133081	C22	-0.279816
C2	-0.511432	H24	0.106234
H2	0.135603	H25	0.105338
CT3	-0.01656	H26	0.106848
CT4	-0.479566	C11	-0.281127
Si2	1.227914	H11	0.104692
C4	-0.501848	H12	0.110457
H4	0.128708	H13	0.103015
C5	-0.497896	C12	-0.289291
H5	0.128431	H14	0.102442
C6	-0.510106	H15	0.103687
H6	0.137179	H16	0.117847

Table 2 Mulliken charges per atom.

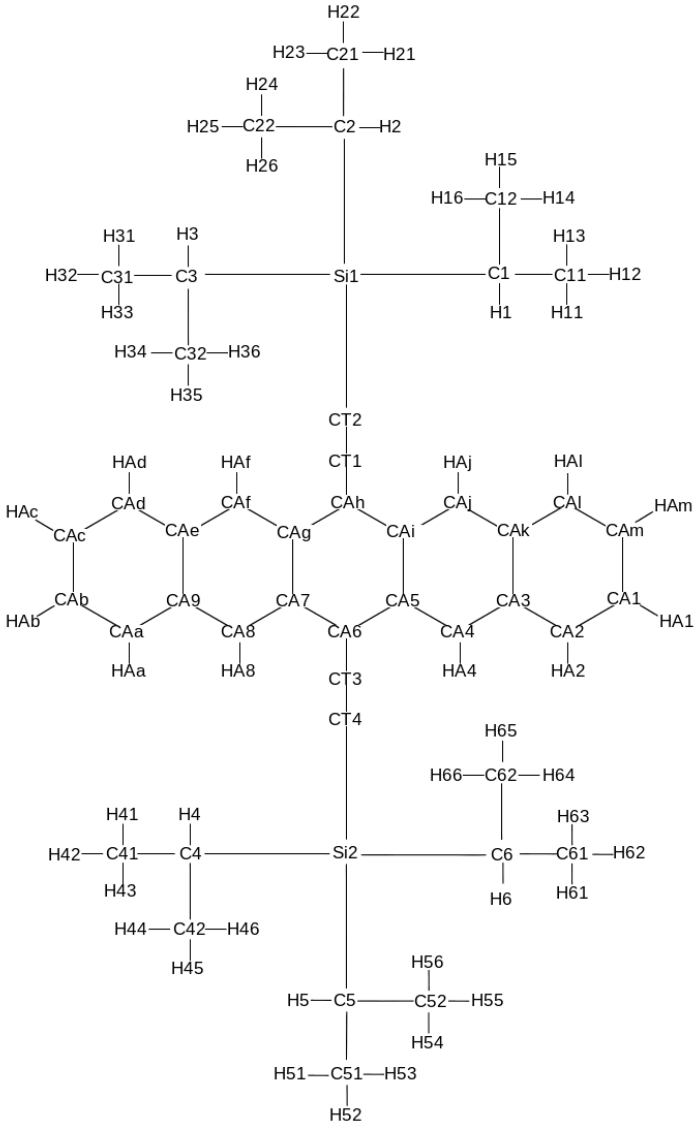

Fig. 1 Molecular structure of TIPS-P with symbols for each atom used for molecular dynamics simulations.

bond	b_0 (nm)	K_b (kJ/mol/nm^2)	source
SI-CT	0.186	132334	from[3]
SI-CZ	0.186	900000	fitted iteratively

Table 3 Bond-specific parameters.

B B. Projective Method versus Molecular Oribital Overlap

In this study, transfer integrals are calculated with the Molecular Orbital Overlap (MOO) method[4]. As discussed by Kirkpatrick, MOO is considerably faster than the projective method since self-consistent density functional theory calculation on the molecular pair can be omitted. MOO is based on the semi-empirical functional ZINDO (Zerner's Intermediate Neglect of Differential Overlap) which can not treat heavy atoms such as silicon.

Replacing silicon with hydrogen and neglecting the rest of the side chains allows the computation of transfer integrals with MOO (see Figure 2b). We belief that this is an appropriate approximation since charge transport occurs between the

angle	θ_0 (°)	K_θ (kJ/mol/rad^2)	source
SI-CT-CT	116.000	488.273	OPLS from CT CT CT
SI-CT-HC	103.500	313.800	OPLS from CT CT HC
CT-SI-CT	134.059	261.217	from[3]
SI-CZ-CZ	179.000	1255.20	OPLS from CT CZ CZ
CT-SI-CZ	105.000	488.273	OPLS from CT CT CZ

Table 4 Angle-specific parameters.

π-systems of TIPS-P which is the pentacene unit. This agrees with the location of the HOMO level (see Figure 2c).

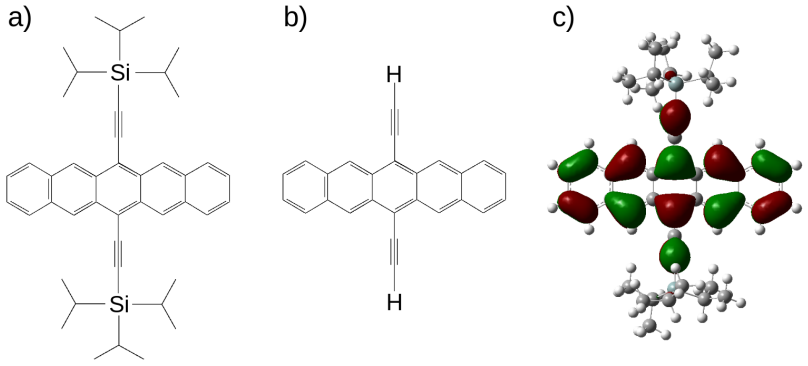

Fig. 2 a) Full molecular structure of TIPS-P and b) simplified structure (right) for transfer integral calculations with MOO. c) HOMO of TIPS-P calculated with the hybrid functional B3LYP and the basis set 6-311g(d,p).

Table 6 compares transfer integrals calculated with the projective method on the full molecular structure of TIPS-P (Figure 2a) and with MOO on the reduced structure (Figure 2b). Transfer integrals computed with MOO are slightly higher than for the projective method. The two-dimensional nature of charge transport in TIPS-P is preserved when calculating transfer integrals with MOO.

C C. Grain Boundaries in TIPS-P as a Network of Small Grains

Wong et al. suggested in reference[6] that grain boundaries in TIPS-P are built from small crystals that are connected to each other by small interfaces. In this section, we study the influence of such a configuration on charge transport. As the interconnectivity between small grains in the grain boundary is unknown, we consider 4 different cases: i) a one-dimensional chain with two connections per grain, ii) a two-dimensional honeycomb structure with three connections per grain, iii) a two-dimensional quadratic lattice with four connections per grain and iv) a two-dimensional hexagonal structure with six connections per grain (see Figure 3a). The distance between next neighbors is set to 1 and model structures are 20 x 20 large.

Each grain is approximated as a hopping-site during charge transport. This assumes that charge transport is limited by grain boundaries and not by the mobility anisotropy within TIPS-P grains (see reference[7]). In our model we consider small interfaces between grains. This allows us to use the results of the previous section for 40 Å wide stripes. For each angle ϑ we computed 20 reduction factors μ_{Xtal}/μ describing the mobility reduction imposed by the grain boundary. Those are randomly assigned to each grain boundary between nano-crystals reducing the hopping rate from one grain to another by the drawn factor μ_{Xtal}/μ.

In terms of charge transport we consider two cases: a) all grains are well connected as if there are no grain boundaries in between them and b) the reduction factor μ_{Xtal}/μ is randomly drawn from all mutual angles [0°,90°]; electrostatic

dihedral	c_1 (kJ/mol)	c_2 (kJ/mol)	c_3 (kJ/mol)	c_4 (kJ/mol)	c_5 (kJ/mol)	c_6 (kJ/mol)	source
CZ-SI-CT-HC	0.76567	2.29701	0.00000	-3.06269	0.00000	0.00000	OPLS from CZ CT CT HC
CZ-SI-CT-CT	0.00000	0.00000	0.00000	0.00000	0.00000	0.00000	from[3]
CZ-CZ-SI-CT	0.00000	0.00000	0.00000	0.00000	0.00000	0.00000	OPLS from alkynes
CT-SI-CT-HC	0.62760	1.88280	0.00000	-2.51040	0.00000	0.00000	OPLS from CT CT CT HC
CT-SI-CT-CT	2.92880	-1.46440	0.20920	-1.67360	0.00000	0.00000	OPLS from CT CT CT CT
SI-CT-CT-HC	0.62760	1.88280	0.00000	-2.51040	0.00000	0.00000	OPLS from CT CT CT HC
CA-CZ-CZ-SI	0.00000	0.00000	0.00000	0.00000	0.00000	0.00000	OPLS form alkynes

Table 5 Dihedral-specific parameters.

vector	$J_{ProjectiveMethode}$ (meV)	J_{MOO} (meV)
a	53.7	85.7
b	0.21	0.71
c	1.17	2.13
a-b	64.8	70.0

Table 6 Transfer integrals calculated with the molecular orbital overlap method (MOO) and the projective method[4]. **a**, **b** and **c** are the unit cell vector of TIPS-P from reference[5]

only and electrostatic and induction are considered. All reduction factors are corrected by the mobility ratio μ_{Xtal}/μ of the complete, 400 x 400 Å^2 structures with parallel grains since this is the case where both grains crystalized, charge transport is unconfined and only disorder within the grain plays a role.

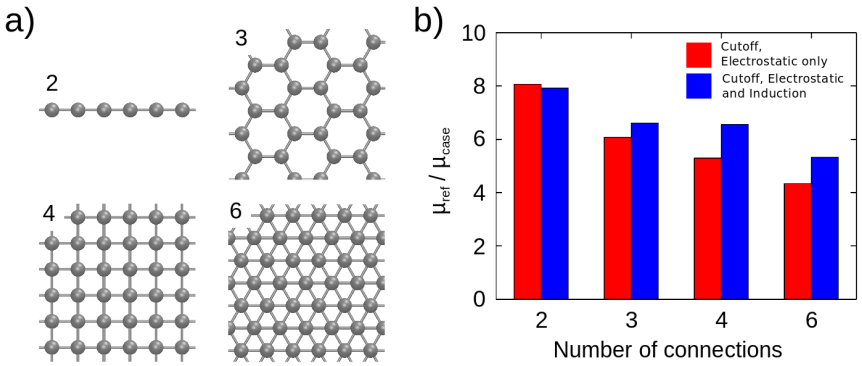

Fig. 3 Grain boundaries as a network of nano-crystals. a) Model for nano-crystals with different connectivity to neighbouring grains. Spheres represent grains and bonds refer to connections between spheres. The number indicates how many next neighbours there are. b) Mobility ratios between a perfectly connected grid μ_{ref} and a network with variation in connectivity μ_{case}. Reduced connection due to grain boundaries are represented by individual (not the average) mobility reductions factors from 4 x 40 nm^2 stipe structures. All angles are considered.

The results of kinetic Monte-Carlo simulations are provided in Figure 3b. Mobilities are calculated from average velocities utilising regenerative contacts. The reference mobility μ_{ref} refers to the case of perfectly connected grains while the mobility μ_{case} relates to the case of reduced connectivity between grains due to small, 4 nm wide grain boundaries (see cases a) and b) from above). The higher the number of connections between grains the lower is the effect of grain boundaries reaching from a mobility ratio μ_{ref}/μ_{case} of around 8 to 4 for two and six connections respectively. More connections allow charge carriers to avoid grain boundaries with a strong blocking effect.

D D. Energy Surface for Varied Mutual Angles

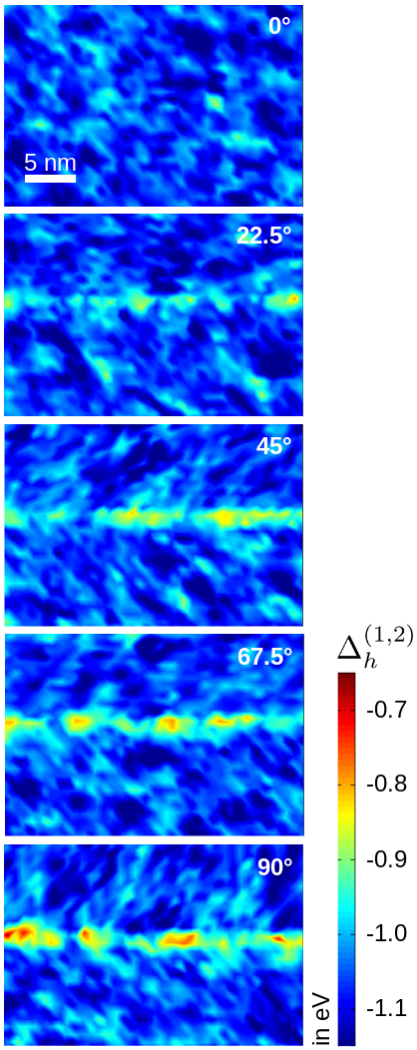

Fig. 4 Energy surfaces of representative two-grain structures for each mutual angle. Energy calculations consider contributions from electrostatics and induction.

E E. Transfer Integral Distribution for Varied Mutual Angles

The effect of varying mutual angle on transfer integrals is shown in Figure 5.

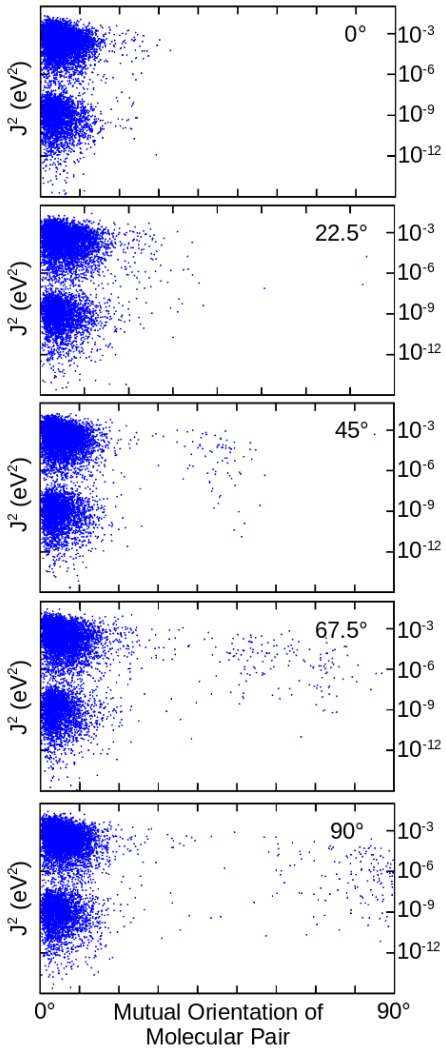

Fig. 5 Transfer integrals calculated for representative two-grain structures for each mutual angle.

F F. Statistics for Two Grains with Varied Mutual Angle

In the main text, charge transport is simulated for large, quadratic structures ($40 \times 40\,nm^2$) and stripes perpendicular to the grain boundary ($4 \times 40\,nm^2$). For large structures, we considered 5 molecular assemblies per angle while we simulated charge transport on 20 stripes per angle. Mobilities resulting from kinetic Monte-Carlo vary. This section aims to quantify this variation. The used metric are mobility ratios of the ideal crystal μ_{Xtal}, the molecular dynamics molecular assemblies without energetic disorder $\mu_{E=const}$ or the molecular dynamics molecular structures with energetic disorder μ (with different cases for site energies).

For the large, $40 \times 40\,nm^2$ structures the standard deviations of the mobility ratios are relatively small compared to the average value (see Figure 6). In contrast, the values of the standard deviations of the mobility ratios for stripes are similar to their average values (see Figure 7). In the case of $\mu/\mu_{E=const}$ standard deviations increase towards large mutual angles. This can be explained by the non-uniform barrier height between grains combined with the increase peak barrier heights for larger mutual angles.

Thus, the average mobility ratio values for large structures are very reliable. Large interfaces between TIPS-P grains

do not seem to impede charge transport. For small inter-granular interfaces charge carrier mobilities are on average more reduced than for large mutual angles. Due to the large standard deviation, charge transport across small grain boundaries might be much better or worse. A simple model, how this variance will affect charge transport in nano-crystalline grain interfaces in TIPS-P is provided in Supporting Information C.

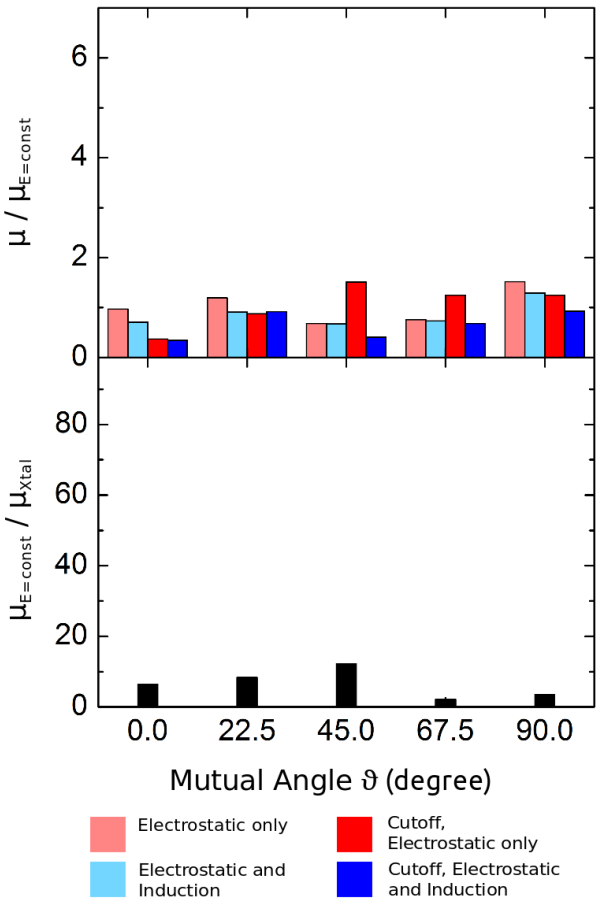

Fig. 6 Standard deviations of mobility ratios for large, 40 x 40 nm^2 structures. μ_{Xtal} refers to the mobility of ideal crystal structure[5], $\mu_{E=const}$ relates to the mobility of the molecular dynamics molecular assembly without energetic disorder and μ is the mobility of the molecular dynamics molecular assembly including energetic disorder considering different cases.

G G. Randomly Grown Multi-Grain Systems of TIPS-P

In the main text, structures with two grains and one linear grain boundary are simulated. Here, we model probabilistically grown, multi-grain structures. Charge transport parameters and charge transport is simulated as described in the main text. Furthermore, we track charge carriers and compute their accumulated occupation time per site allowing for a characterisation of the general charge transport behaviour in multi-crystalline films of TIPS-P.

Molecular assemblies are initially prepared with an algorithm probabilistically simulating the growth of grains. At first, the number of grains is chosen. Accordingly, seeds are randomly placed on a two-dimensional surface. Seeds are molecules that are oriented with 0, 22.5, 45, 67.5 or 90 degrees compared to the **a**-vector of the TIPS-P unit cell. Grains can grow in the **a** and **b** direction of the TIPS-P crystal structure. The initial seeds are the first generation of molecules. For every following generation, the probability to grow is reduced by a factor of 10 ensuring grains of similar size. The code avoids overlapping of molecules when one grain reaches another one. The process of placing molecules is repeated until a predefined number of molecules has been placed. Accordingly, the molecular assemblies are equilibrated with atomistic molecular dynamics as described in the main text for two-grain systems. An example structure is provided in Figure 8a.

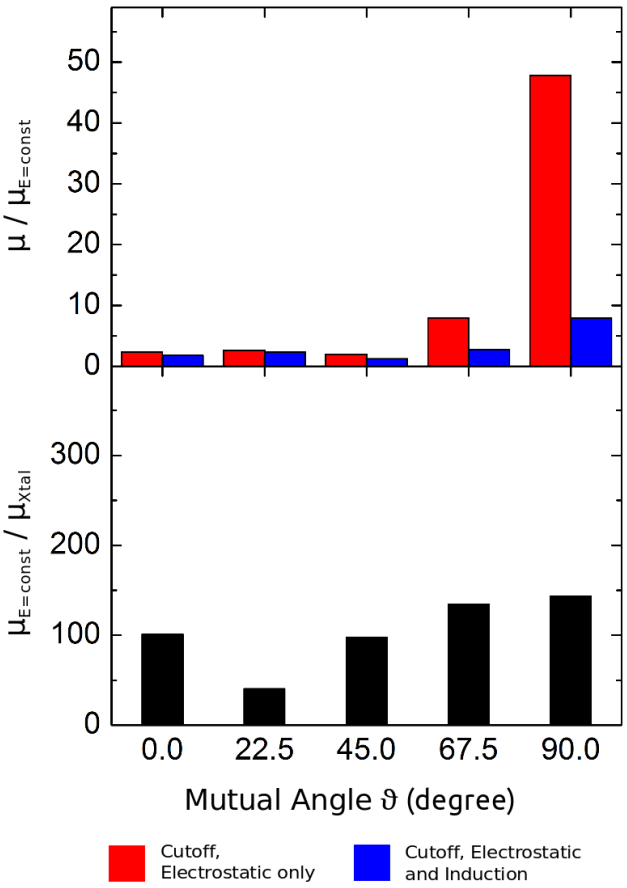

Fig. 7 Standard deviations of mobility ratios for 4 x 40 nm^2 stripes. μ_{Xtal} refers to the mobility of ideal crystal structure[5], $\mu_{E=const}$ relates to the mobility of the molecular dynamics molecular assembly without energetic disorder and μ is the mobility of the molecular dynamics molecular assembly including energetic disorder considering different cases.

The energy surface referring to calculations including electrostatics and induction is depicted in Figure 8b. Energy barriers between grains are particularly high for interfaces with large mutual angle. Moreover, we observe high potential energies for hole transport when three grains join each other. This is not surprising as the multipole moments of the three grains are not aligned. Additionally, voids distort the energy surface and significantly influencing the site energies of adjacent molecules. As mentioned previously, the energy barriers are non-uniform and allow charge carriers to cross at reduced energy cost.

Figures 8c and d show accumulated occupation times of charge carriers during 1 s of charge transport. The orientation of the applied electric field F indicates the direction of charge transport. Dark blue areas relate to regions where no charge transport happens. Yellow and red areas refer to molecules where charge carriers are blocked from traveling. Bright blue areas are regions where good charge transport occurs. This is mainly the case within grains. We observe that charge transport is impeded by large barriers, at regions where three grains join each other and at voids.

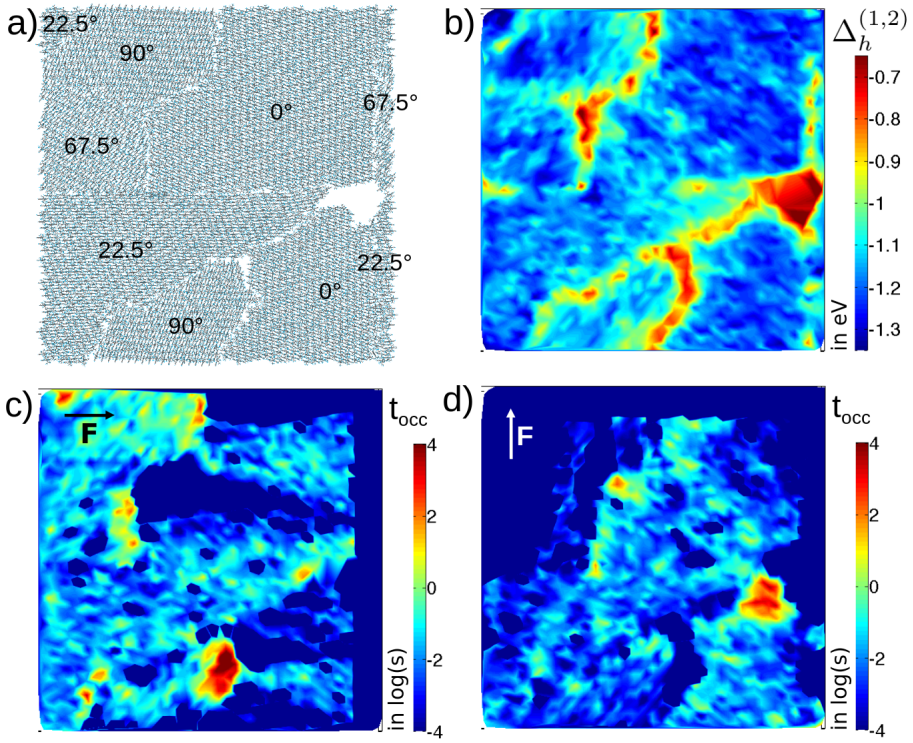

Fig. 8 Charge transport in multi-grain structures of TIPS-P. a) Equilibrated molecular dynamics structure, b) energy surface calculated including contributions of electrostatics and induction, c) and d) accumulated occupation times during 1 s of charge transport simulations. The orientation of the electric field F indicates the direction of charge transport.

H H. Alternative Representation of Transport Data

In this section, average mobilities are obtained using mobility ratios that are flipped compared to the main paper. This effectively means considering the average conductance rather than the average resistance. In a networked granular system of unknown structure, it is not definite which average woudl be nmore appropriate. In the case, we do not observe a clear trend towards larger angles. In the representation of Figure 3b in the main text, the average was dominated by few, large mobility reductions. The effect of those outliers are less pronounced when inverting the mobility ratios (see Figure 10).

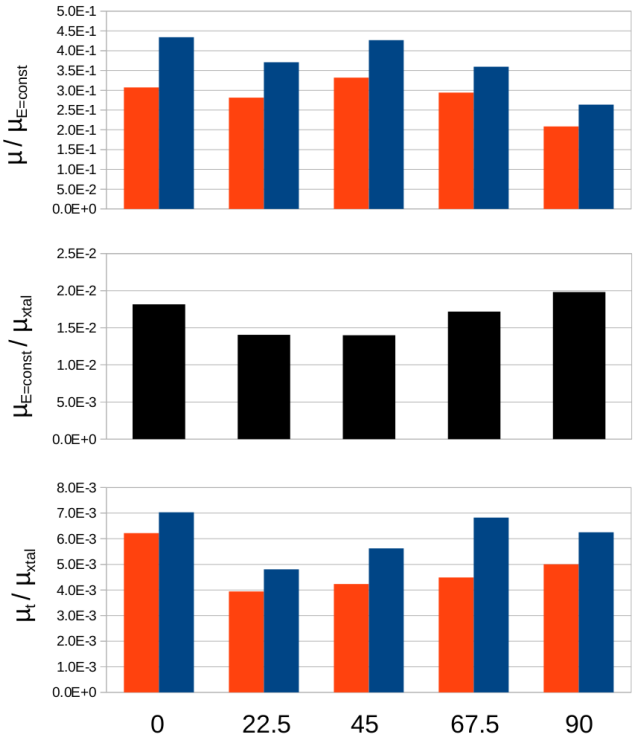

Fig. 9 Average mobility ratios for large 40 x 40 nm^3 structures. Mobility ratios are flipped compared to Figure 3a.

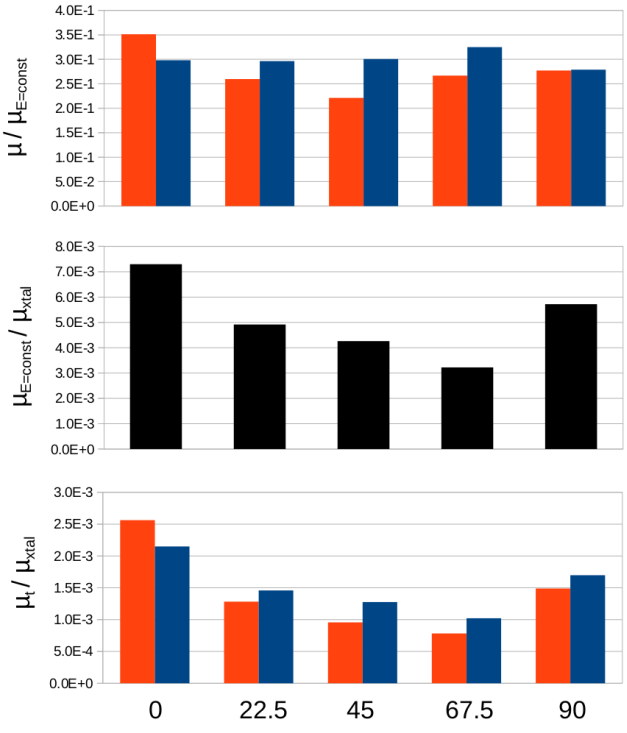

Fig. 10 Average mobility ratios for large 4 x 40 nm^3 structures. Mobility ratios are flipped compared to Figure 3b.

References

1 W. L. Jorgensen, D. S. Maxwell and J. Tirado-Rives, *J. Am. Chem. Soc.*, 1996, **118**, 11225–11236.

2 J. C. G. Pereira, C. R. A. Catlow and G. D. Price, *The Journal of Physical Chemistry A*, 2002, **106**, 130–148.

3 A. A. Y. Guilbert, J. M. Frost, T. Agostinelli, E. Pires, S. Lilliu, J. E. Macdonald and J. Nelson, *Chemistry of Materials*, 2014, **26**, 1226–1233.

4 J. Kirkpatrick, *Int. J. Quantum Chem.*, 2008, **108**, 51–56.

5 J. E. Anthony, J. S. Brooks, D. L. Eaton and S. R. Parkin, *J. Am. Chem. Soc.*, 2001, **123**, 9482–9483.

6 C. Y. Wong, B. L. Cotts, H. Wu and N. S. Ginsberg, *Nature communications*, 2015, **6**, year.

7 J. Wade, F. Steiner, D. Niedzialek, D. T. James, Y. Jung, D.-J. Yun, D. D. Bradley, J. Nelson and J.-S. Kim, *Journal of Materials Chemistry C*, 2014, **2**, 10110–10115.